Dialkylamide as both capping agent and surfactant in a direct solvothermal synthesis of magnetite and titania nanoparticles

Claudio Cara,[ab] Anna Musinu,[ac] Valentina Mameli,[a] Andrea Ardu,[ac] Daniel Niznansky,[d] Josef Bursik,[e] Mariano A. Scorciapino,[f] Giorgia Manzo, [f]Carla Cannas*,[abc]

[a]Department of Chemical and Geological Sciences, Università di Cagliari, S.S. 554 bivio per Sestu, 09042, Monserrato (CA), Italy

[b]Consorzio AUSI, Palazzo Bellavista Monteponi, 09016 Iglesias, CI, Italy

[c]INSTM, Cagliari Unit

[d]Department of Inorganic Chemistry, Charles University of Prague, Czech Republic

[e]Institute of Inorganic Chemistry, Czech Academy of Science, Rez, Czech Republic

[f]Department of Biomedical Sciences, Biochemistry Unit, University of Cagliari, Italy

*Address correspondence to

Carla Cannas: ccannas@unica.it

KEYWORDS

One-pot synthesis, magnetite nanoparticles, solvothermal method, capping agent, dialkylamide, surfactants role, oleic acid, oleylamine

ABSTRACT

An eco-friendly, low-cost, one-pot solvothermal approach has been developed to prepare spherical magnetite nanoparticles with sizes in the 7-12 nm range capped with a dialkylamine. Iron isopropoxide, water vapour, absolute ethanol, oleic acid and oleylamine were used as iron oxide precursor, hydrolysis agent, solvent and surfactants, respectively. The surfactants' role was investigated and an accurate correlation among the synthetic parameters, the crystallographic phases and both crystallite and particle size was found. The amounts of oleylamine and oleic acid and the temperature have been revealed to be the key parameters in order to tune particle size and their polydispersity. An in-depth study on the role of each surfactant has pointed out the fundamental role of the amine as reduction promoter as demonstrated by using different amines and confirmed by

Mössbauer measurements. A dual ^{1}H-NMR-FTIR approach on selected experiments for the investigation of the capping agents (in the presence of a magnetic phase (Magnetite) or a diamagnetic one (Anatase) prepared in the same synthetic conditions) has been found to be fundamental to clarify the actual nature of the capping agent of the nanoparticles and the reactions involved between the-surfactants. New insights on the reaction mechanism confirm the formation of an amide that represents a new co-surfactant for the size and shape regulation and a biocompatible molecular coating of magnetite and anatase nanoparticles.

INTRODUCTION

Solvothermal syntheses can be commonly defined as all those strategies based on chemical processes performed in a closed vessel (autoclave) above ambient temperature and pressure.[1,2] Under specific pressure (typically between 1 and 10,000 atm) and temperature (typically between 100 °C and 1000 °C) the interaction of precursors during the synthesis is highly facilitated.[3] If water is used as the solvent, the method is called “hydrothermal synthesis”. The nature of the reagents and solvents, as well as temperature and pressure, are key parameters for the synthesis of inorganic materials. For a long time used for bulk materials, solvothermal and hydrothermal approaches have recently become more and more appealing due to the possibility to synthesize nanosized materials with well-defined size and morphology by means of suitable surfactants in non-aqueous[4–6] or in water-alcohol media.[7–9] The growing interest for these strategies derives from the lower toxicity and the lower cost of the solvents that can be employed, when compared to those commonly used in widely diffused surfactant-assisted non-aqueous hot injection[10–15] and heating-up processes.[15–19] Other advantages include the possibility to use moderate reaction temperatures, the low boiling point of the solvents and the high repeatability of the synthesis. These advantages render solvothermal processes promising low cost, eco-friendly and reliable strategies for the synthesis of inorganic nanostructures. Various examples of their use in the presence of surfactants for the synthesis of metal oxide nanostructures such as magnetite,[4,20] hematite,[21,22] cobalt ferrite,[8,9] ceria,[23] zinc oxide,[24] titania[5,6] are reported in the literature. Among the different strategies proposed, the one developed by Dinh et al. for titania[5] is extremely promising because of the fine control of both size and shape of the nanoparticles.

Nanostructured iron oxides, in particular maghemite and magnetite are the most useful systems for technological applications, from high-density storage,[25] to catalysis,[26–28] gas-sensing and pollutant removal.[29–31] Furthermore, being approved by US Food and Drug Administration,[32] iron oxides have attracted great interest also for their applications in biomedicine,[32–37] from drug delivery to diagnostics and therapy (theranostic).[38] Although in the literature a number of synthetic approaches

have been proposed both in water and non-aqueous media, the last ones are the most promising because of a better control on particle size, size distribution, shape and a higher degree of crystallinity of the final product.[1,15,16,18,39] In these strategies the surfactants (commonly oleic acid and/or oleylamine) play a key role on the control of nucleation and growth kinetics, on the stabilization of the colloidal nanoparticles and, sometimes, it has been reported their role as solvents[40,41] and as reducing agents.[42–44] Despite the great interest and the numerous publications in this field, just a few works are devoted to the investigation of chemical reactions of the organic species involved during the formation of inorganic nanoparticles and their transformation during the synthesis.[42,45]

This work represents a new contribution to the synthetic solvothermal approach, as well as to the understanding of the reaction mechanism involved in the formation of the iron oxide (magnetite, M; hematite, H) nanoparticles and of their molecular coating. Novel insights on the role of the surfactants and the nature of the capping agent were obtained. Indeed, oleic acid (OAc) and oleylamine (OAm) are commonly found as the capping agents in the colloidal dispersions of inorganic nanoparticles (metals, metal oxides, sulphides). In our synthetic conditions, oleic acid and oleylamine react to form a dialkylamide that has been found the only capping agent bound at the nanoparticle surface. Furthermore, it has been demonstrated that the amine group has a fundamental role in the Fe^{III}-Fe^{II} reduction for the formation of magnetite nanocrystals.

EXPERIMENTAL

Chemicals. FeIS was synthesized by the reaction between potassium iso-propoxide and iron (III) chloride. For further details see the Supporting Information (SI_1). Oleic Acid (OAc, 90%), Oleylamine (OAm, 70%), Absolute Ethanol (99.9%), Ethanol (96.4%), Cyclohexane (>99%), Octylamine (OcAm, 99.5%), Butylamine (BuAm, 99.5%), Titanium Iso-propoxide (TiIS, 97%), deuterated Cyclohexane-d12 (99.6 atm.% D) and Ethanol-2,2,2-d3 (99.0 atm.% D) were purchased from Sigma-Aldrich and used as received.

Synthesis of iron oxide nanoparticles. Hydrophobic capped magnetite nanoparticles with sizes in the 7-12 nm range were synthesized as follows. Inspired by the synthetic strategy proposed by Dinh et al.[5] for titania nanoparticles, Iron(III) iso-propoxide (FeIS), water vapour and absolute ethanol, were used as iron oxide precursor, hydrolysis agent and solvent, respectively. Oleylamine (OAm) and Oleic acid (OAc) were used as surfactants to control the nucleation and growth of the nanoparticles. The synthesis was carried out within an autoclave made of a closed stainless steel vessel with a Teflon internal jacket and lid and a smaller Teflon container placed in the centre

(SI_2). The outer compartment held the hydrolysis agent (ethanol-water azeotropic mixture; ethanol 96,4%) whereas the mixture of iron alkoxide, surfactants and absolute ethanol was kept within the inner Teflon beaker. Iron alkoxides commonly form amorphous iron hydroxy- or oxyhydroxy-phases due to their high reactivity in the presence of liquid water. In order to obtain crystalline nanoparticles, a further step of thermal treatment is necessary without the possibility to control phase, size and shape. Conversely, these features can be regulated by inducing a decrease of the hydrolysis rate through the use of the ethanol-water azeotropic mixture and of FeIS. In a typical synthesis, a mixture of FeIS, surfactants and absolute ethanol (see Table1) was magnetically stirred for 20 minutes, transferred into the inner Teflon beaker and finally placed inside the autoclave. Then, the outer jacket was filled with 17 mL of ethanol (96.4%). The sealed autoclave was inserted into an oven and kept at a selected temperature for 18 hours. The nanoparticles (NPs) were separated from the supernatant by centrifugation at 4500 rpm for 15 minutes, washed with 5 mL of ethanol, centrifuged at 4500 rpm for 15 minutes and finally dispersed in 10 mL of cyclohexane. The as-obtained colloidal dispersions were stable for months. The supernatant and the washing solutions were collected for the FTIR and NMR analyses.

In order to investigate on the role of the capping agent, five samples were prepared: without any surfactant (H_NS), in the presence of either Oleic Acid (H_OAc) or Oleylamine (M_OAm) or a mixture of them with a FeIS:OAm:OAc ratio equal to 1:6:4 (M1_OAm_OAc) or 1:30:20 (M2_OAm_OAc), where H and M in the labels stem for Hematite and Magnetite phases. An additional sample was prepared in the absence of the hydrolysis agent (ethanol-water azeotropic mixture) in the external compartment (M3_OAm_OAc).

Five samples of magnetite nanoparticles were synthesized at different temperatures (140 °C, 160 °C, 180 °C, 200 °C, 220 °C) to study in depth how this parameter affects their final morphology and size. All the syntheses were carried out by using a molar ratio FeIS:OM:OA equal to 1:30:20 as for the sample M2_OAm_AOc (M2_T180). The samples were labelled as M2_TX (X=140, 160, 180, 200, 220). The maximum temperature is dictated by the use of Teflon as material for the synthesis containers.

To clarify the role of the amine in the Fe^{III}-Fe^{II} reduction process, three samples (M2_OAm, M2_OcAm, M2_BuAm) were prepared in the presence of different amines (Oleylamine (OAm), Octylamine (OcAm) and Butylamine (BuAm)) with FeIS:Am 1:1 molar ratio, and other two in the same conditions of M2_OAm_OAc but using Butylamine (M2_BuAm_OAc) instead of Oleylamine (M2_OcAm_OAc). Table 1 summarizes the details of the syntheses.

Synthesis of anatase nanoparticles. Rhombic shaped anatase nanoparticles (A_OAm_OAc) were prepared in the same synthetic conditions of the sample M2_OAm_OAc (see Table 1) using titanium iso-propoxide, oleylamine, oleic acid and absolute ethanol as the metal precursor, the surfactants and the solvent, respectively. A in the label stems for Anatase phase.

Characterization techniques. The samples were characterized by X-ray Diffraction (XRD), using a Seifert instrument with a θ-θ Bragg-Brentano geometry with Cu-Kα wavelength. The mean size of the crystalline grains (<D_{XRD}>) was computed by means of the Scherrer equation and adopting the Warren correction. The curve-fitting procedure was carried out on the most intense X-ray peaks ({220}, {311}, {400}, {440}) by means of Origin Software using the PseudoVoigt function. The <D_{XRD}> values were determined as the average among the different reflections with the associated standard deviation. For the Transmission Electron Microscopy (TEM) observations, the stable cyclohexane magnetite dispersions were directly dropped on carbon-coated copper grids. The as-prepared samples were observed in electron micrographs obtained with a TEM (JEOL 200CX), operating at 200 kV. The particle size distribution on bright field images and the mean particle size (<D_{TEM}>) were determined by means of three different methods, considering the nanoparticles as spheres: manual, automatic by ImageJ software[46] and automatic by PEBBLES software[47]. Results are shown in the Supporting Information (SI_3). Here, only the results obtained by means of PEBBLES are shown, being the most reliable data when compared with those obtained by manual determination mode by ImageJ. The polidispersity index was calculated according to the following equation:

$$Standard\ deviation\ s.d.\% = \frac{\sqrt{\frac{\sum_{i=1}^{N}(x_i-\bar{x})^2}{N-1}}}{\bar{x}} \times 100$$

where $\bar{x}$ is the mean value and x_i represents the i-th diameter value.

High-resolution TEM (HRTEM) images were obtained by using a JEOL JEM 2010 UHR equipped with a Gatan Imaging Filter (GIF). Fourier Transformed Infrared (FTIR) spectra were collected in the region from 400 to 4000 cm^{-1} by using a Bruker Equinox 55 spectrophotometer. Capping agents and samples (as colloidal dispersions) were analysed by placing a drop of the liquid on the top of a KBr pellet.

The Mössbauer spectra were done in the transmission mode with ^{57}Co diffused into a Rh matrix as the source moving with constant acceleration. The spectrometer was calibrated by means of a standard α–Fe foil and the isomer shift was expressed with respect to this standard at 293 K. The samples were measured at the temperature of 293 K. The fitting of the spectra was performed with the help of the NORMOS program.

Nanoparticles washing solution were studied by means of Nuclear Magnetic Resonance (NMR) spectroscopy. In the case of diamagnetic nanoparticles, spectra were acquired also on their cyclohexane dispersion. Samples (600 μL + 100 μL of the deuterated solvent) were loaded in 5.0 mm NMR tubes, and ^{1}H spectra were acquired with a Unity Inova 500NB high-resolution spectrometer (Agilent Technologies, California, USA) operating at a frequency of 500 MHz. Experiments were carried out at 300 K. Depending on the solvent, chemical shifts were referenced to the ethanol CH_3 triplet (1.11 ppm from trimethylsilane (TMS)) or cyclohexane singlet (1.38 ppm from TMS) before solvent suppression. The latter was achieved by application of the WET sequence,[48,49] which uses a combination of shaped selective excitation and pulsed field gradients. The 'seduce' or 'uburp' pulse shape was used for multiple- and single-resonance suppression, respectively. ^{1}H spectra were acquired using a 6.6 μs pulse (90°), 1.0 s delay time, 1.5 s acquisition time, and a spectral width of 6.65 kHz. ^{1}H-^{1}H correlation COSY spectra were recorded over the same spectral window using 2048 complex points and sampling each of the 256 increments with 32 scans. The same acquisition parameters were applied, together with a mixing time of 200 ms for the acquisition of NOESY spectra.

RESULTS AND DISCUSSION

Role of the surfactants. In order to investigate on the role of each surfactant, different samples were prepared in the absence of the two surfactants, in the absence of oleylamine, in the absence of oleic acid and with different FeIS:(OAm+OAc) ratios, and the results in terms of microstructure and morphology are here reported. XRD patterns in Figure 1 reveal the presence of hematite as a single phase (Space group $\boldsymbol{R\bar{3}c}$, PdF card N. 330664) in the absence of any surfactant (H_NS) as well as in the presence of oleic acid (H_OAc). A unique spinel phase (magnetite, space group $\boldsymbol{Fd3m}$, PdF card N. 190629; maghemite, space group $\boldsymbol{P4_132}$, PdF card N. 391346), is observed when oleylamine (M_OAm) or suitable mixtures of oleylamine and oleic acid (M1_OAm_OAc and M2_OAm_OAc) are used (Figure 1). The samples H_NS and H_OAc are red-brownish coloured confirming the presence of the hematite phase, whereas the samples M_OAm, M1_OAm_OAc and M2_OAm_OAc are black, suggesting the formation of magnetite. TEM images of the samples are shown in Figure 2. The sample H_NS is characterized by the presence of large spheroidal aggregates (100-500 nm) made up of nanoparticles of about 25 nm in size together with small particles of about 6 nm in size. As expected, in the absence of any surfactant it is not possible to control both size and shape of the particles (Figure 2a and inset). In the presence of oleic acid (H_OAc) the product is mainly made of particles with squared platelet shape of about 100 nm (Figure 2b and inset). High resolution TEM (Figure 2c) confirms the formation of hematite, as

evidenced by the lattice parameter of 2.52 Å associated to [110] planes. The peculiar features of the hematite nanoparticles suggest that oleic acid strongly interacts with specific hematite faces favouring the growth of the non-interacting planes, as reported by other authors.[50] When oleylamine is used as unique surfactant (M_OAm), small magnetite nanoparticles of about 4-6 nm are obtained with diverse shapes (Figure 2d). The addition of oleic acid in a suitable ratio with iron (III) iso-propoxide (FeIS) and OAm (FeIS:(OAm+OAc) = 1:10) produces a similar effect (M1_OAm_OAc). However, in this case the average distance among the particles is more regular (Figure 2e). In Figure 2f High Resolution TEM shows two particles with a triangular and a hexagonal shape respectively. They confirm the formation of magnetite, as evidenced by the vales of the lattice planes (2.1 Å -[400], and 2.5 Å -[311]). A decrease in the FeIS:(OAm+OAc) ratio from 1:10 to 1:50 (M2_OAm_OAc) leads to the formation of spherical monodisperse magnetite nanoparticles that self-assemble into a monolayer when deposited on a TEM-grid (Figure 2g), due to the low polydispersity, the regular shape. A detail of a single spherical nanoparticle observed by High Resolution TEM (Figure 2h) and the relative FFT image (inset) confirm the presence of magnetite crystalline phase in agreement with XRD data. The differences in the nanoparticles shape could be explained taking into account both the affinity of the surfactant molecules to specific nanocrystal faces and the FeIS:surfactants ratio. When the FeIS:surfactants ratio is equal to 1:10, nanoparticles with different shapes are obtained. This could be justified hypothesizing that the amount of surfactant molecules is not sufficient to completely surround the nanoparticle's surface, and due to the selective affinity to some lattice planes, the growth along certain directions can be inhibited leading to the formation of particles with anisotropic shape (triangular or hexagonal). Conversely, when the ratio is 1:50, the probability of interaction of the surfactants with the other lattice planes increases and an isotropic shape is obtained.

Effect of the hydrolysis agent. A further experiment without the use of the hydrolysis agent (water vapour deriving from the ethanol azeotropic mixture) was performed (M3_OAc_AOm, Table 1). XRD analysis (Figure 1) indicates the presence of magnetite as unique nanophase. TEM micrograph of the sample (M3_OAm_OAc) prepared in the absence of the external azeotropic mixture (Figure 2i) evidences the presence of diverse shaped nanoparticles pointing out that the water vapour is essential to better control the hydrolysis and condensation reactions of the iron alkoxides and to achieve samples with spherical and monodispersed sizes as for M2_OAm_OAc sample.

Effect of the reaction temperature. In Figure 3a XRD patterns of the samples synthesized at different temperatures (from 140°C to 220°C) show the presence of a unique spinel phase associated to magnetite. The mean size of crystalline grains (<D_{XRD}>) increases with increasing temperature (Table 2). TEM images are reported in Figure 3b. Nanoparticles synthesized at the lowest temperature (M2_T140) are characterized by a spheroidal shape with a broad particle size distribution (Figure 3c, Table 2). At 160 °C nanoparticles become spherical-shaped and a significant improvement of the size distribution is observed (polydispersity lower than 10%). A linear trend of crystalline grain size (<D_{XRD}>) as a function of the reaction temperature has been found and the same tendency is confirmed for particle size (<D_{TEM}>) by TEM analysis, as shown in Figure 3d. The differences between <D_{XRD}> and <D_{TEM}> are expected being <D_{XRD}> the average coherent domain size and <D_{TEM}> the average particle size obtained by bright field images.

Role of the oleylamine in the reduction reaction. Although oleylamine is the most common surfactant used for the synthesis of inorganic nanoparticles, its role is not yet fully understood. In the literature some authors state that oleylamine may act as reducing agent besides as solvent, as size and shape regulator and as stabilizer.[40–44] Other authors ascribe the function of reducing agent to solvents like alcohols.[7] Moreover, two recent works report reactions between alcohols and amines for amide bond formation in the presence of suitable catalysts.[51,52] In our synthetic conditions, when the synthesis is performed in the absence of Oleylamine, the Fe^{III}-Fe^{II} reduction process resulted to be inhibited, being hematite the only phase formed (H_NS and H_OAc).[53,54] Conversely, a black powder with spinel phase (magnetite) forms only when Oleylamine is used alone or together with Oleic Acid. Thus, the amine functional group appears to be somehow responsible for the reduction reaction. In order to ascertain the role of the amine group in the reduction process, different amines (without unsaturation and with different length of the hydrocarbon chain) were alternatively used and the final product analysed (Table 1). Three samples (M2_OAm, M2_OcAm, M2_BuAm) were synthesized only in the presence of an amine (Amine (Am), Oleylamine (OAm), Octylamine (OcAm); Butylamine (BuAm), with a FeIS:Am ratio of 1:1. The colour of all the colloidal dispersions, as well as the XRD patterns (Figure 4a) suggest the formation of magnetite nanoparticles with similar crystallite sizes (4.0 ± 0.3 nm) (see also SI_4 for TEM analysis). A small amount of the Amine (Am) (FeIS:Am = 1:1) results sufficient to promote the Fe^{III}-Fe^{II} reduction and to obtain magnetite phase but it does not ensure colloidal and chemical stability over time. Indeed, the inorganic phase, being poorly capped, changes its colour to brownish probably because of the oxidation to maghemite. Moreover, when the length of the hydrocarbon chain is reduced, the nanoparticles appear more agglomerated (SI_4a; SI_4b). Not surprisingly, this

effect is much more evident for the sample synthesized in the presence of BuAm. Two more samples were prepared in the same conditions of M2_OAm_OAc (FeIS:(OAm:OAc) = 1:30:20) but using Butylamine (M2_BuAm_OAc) or Octylamine (M2_OcAm_OAc) instead of Oleylamine. These results indicate that a better control on the particle size and shape can be reached only by the addition of Oleic Acid (SI_4c; SI_4d) to the amine leading in all the cases to the formation of bigger crystallites (from about 4 nm to about 7 nm). Moreover, these samples retain the typical black colour of magnetite and appear stable for months. Although the XRD has been used to identify the crystalline phase, the patterns cannot be univocally assigned to Fe_3O_4 (magnetite, $Fe^{II}Fe^{III}_2O_4$) rather than γ-Fe_2O_3 (maghemite, $Fe^{III}_2O_3$) because these crystalline phases are isostructural. In order to prove the Fe^{III}-Fe^{II} reduction and the formation of magnetite, ^{57}Fe Mössbauer Spectroscopy has been used. Figures 4b and 4c show the Mössbauer spectra collected at room temperature of the sample M2_OAm_OAc and M2_BuAm_OAc. The spectra show two sharp sextets and broad singlets. Mössbauer parameters are reported in Table 3. For the sample M2_OAm_OAc the first sextet (Isomer Shift 0.26 and Hyperfine Field 48.8) corresponds to Fe^{III} in tetrahedral position in magnetite, the second one (Isomer Shift 0.68 and Hyperfine Field 45.7) corresponds to Fe^{III} and Fe^{II} in octahedral position in magnetite as well. The ratio of the areas of the two sextets (A_{Sext1}:A_{Sext2}) is equal, within the experimental error, to 1:2. These findings allow to unambiguously state that magnetite is present as a ferrimagnetic phase in the observed sample.[55,56] Very similar features are exhibited by the sample prepared with Butylamine confirming the fundamental role of the amine group in the Fe^{III}- Fe^{II} reduction (Table 3). In the spectra we can also observe the presence of broad singlets with an isomer shift of about 0,36 which could be attributed to Fe^{III} in a non-ordered/superparamagnetic state. This observation is in agreement with XRD and TEM data: particle size and crystal size being different of about 2 nm. The difference can be therefore associated to a disordered phase that could form at the surface creating a core shell structure with a magnetite core. However, internal disorder cannot be excluded.[57]

Study of the capping agent

The present study has shown that a mixture of oleic acid and oleylamine in a suitable ratio with the iron precursor (FeIS:OAm:OAc = 1:30:20) ensures the production of spherical magnetite nanoparticles with low polydispersity. Chemical reactions involving organic molecules play an outstanding role in the surfactant-assisted non-aqueous media synthesis of inorganic nanoparticles, though it has not been fully understood.[1] In order to investigate the organic reactions involved in our synthetic process, a combined ^{1}H-NMR and FTIR study has been carried out. Since colloidal dispersions of magnetite nanoparticles could not be analyzed by NMR spectroscopy due to the extreme signal broadening caused by their ferrimagnetic properties, suitable nanoparticles of a

diamagnetic oxide (titania in the anatase phase, A_OAm_OAc) has been synthesized under the same experimental conditions. XRD (SI_5) and TEM data of the sample A_OAm_OAc indicate the presence of anatase as unique phase and a rhombic shape of the nanoparticles (Figures 5c and 5d). Magnetite and anatase colloidal dispersions (Figures 5a,b,c,d) washed with ethanol (M2_OAm_OAc and A_OAm_OAc) have been first analysed through FTIR (Figure 5e) and the results compared to those acquired on the washing solutions (W_M2_OAm_OAc and W_A_OAm_OAc, respectively). The simple mixture of oleic acid and oleylamine prepared at room temperature (OAm_OAc) has been reported as a reference.

The spectra of the colloidal suspensions M2_OAm_OAc and A_OAm_OAc and of the washing solutions W_M2_OAm_OAc and W_A_OAm_OAc, are very similar, indicating the presence of the same organic species. The only remarkable difference is the large band in the 500-700 cm^{-1} range associated to the Me-O stretching of the inorganic metal oxide (SI_6[58–63]) in the dispersions. The bands in the 1400-1700 cm^{-1} range (SI_6) together with the band at 3295 cm^{-1} suggest the presence of an amide both in the magnetite and the anatase dispersions as well as in their washing solutions. The amide can be produced by the condensation reaction between oleic acid and oleylamine. Water, the byproduct of the condensation, is then available for the hydrolysis of the iron alkoxide used for the nanoparticle synthesis. This is consistent with the results of the experiment (M3_OAm_OAc, Figure 1 and Figure 2i) performed without the use of the azeotropic mixture in the external compartment, that indicates that capped magnetite nanoparticles is formed anyway.

In order to confirm the amide formation and to clarify if the species is the only capping agent of the nanoparticles, ^{1}H-NMR was the method of choice. Spectra are shown in figure 5f: chemical shift values together with resonances multiplicity and relative integrated areas are reported in Table 4. As expected, only the resonances from oleic acid and oleylamine are detected in the spectrum of OAm_OAc. The CαH_2 resonance of both the species in the mixture is observed to significantly shift when compared to the corresponding signal recorded from the two separately dissolved in ethanol (SI_7). This is due to their acid-base interaction, resulting in the formation of the corresponding ionic species, as observed also in other solvents like cyclohexane[64] and $CDCl_3$.[59] Beside the resonance of oleylamine, those attributable to a N-alkylamide are observed in the spectrum of the samples W_M2_OAm_OAc, W_A_OAm_OAc and A_OAm_OAc. The amide has been unequivocally identified on the basis of: i) the appearance of a resonance at ~7.9 ppm, which is in the typical amide protons region; ii) this resonance shows a triplet fine-structure clearly due to the scalar coupling with the CH_2 bonded to the nitrogen, which is typically not resolved in the free amine; iii) the appearance of two additional resonances in the CαH_2 region, one triplet slightly shifted to lower frequency with respect to the resonance of oleic acid when separately dissolved in

ethanol, one multiplet significantly shifted to higher frequency then the oleylamine; iv) the fine structure of the latter has been solved to be a doublet of triplets compatible with the N-alkylamide; v) in the COSY spectra (SI_8b), the new triplet shows the same cross-peaks pattern as the oleic acid, the new multiplet as the oleylamine (the above mentioned scalar coupling generating the fine-structure of the amide proton has been also confirmed from COSY); vi) the NOESY (SI_8a) unequivocally shows correlation of both these two new resonances with that of the amide proton. Finally, in the ^{1}H-NMR spectrum of the colloidal dispersion of anatase nanoparticles (Figure 5f), only the resonances due to the N-alkylamide were observed, confirming this species as the only capping agent. The amide proton resonance (**H**N amide) was found to dramatically shift to lower frequency (from about 7.90 ppm in the washing solutions to 7.46 ppm in the anatase dispersion) respect to the same signals of the free amide in the washing solutions (W_A_OAm_Oac, W_M2_OAm_OAc). Conversely, the Cα**H**$_2$-NH and Cα**H**$_2$-CO amide protons do not undergo significant modifications, being the differences within the experimental error (Table 4). These findings strongly suggest that the amide is bound at the surface of anatase nanoparticles through the amide proton (NH) probably via hydrogen bond, while oxygen and nitrogen are not directly involved. Taking into account the great similarities of the FTIR data on M2_OAm_OAc and A_OAm_OAc dispersions, it can be assumed that also magnetite nanoparticles are capped with the same N-Alkylamide (Figure 6). Some authors in rather different synthetic conditions (microwave synthesis, aqueous solutions and in the presence of HCl) report a similar reaction but they declare that the dialkylamine (dioleamide) is formed only in the presence of gold nanoparticles as catalyst of the condensation reaction between Oleic Acid and Oleylamine.[65]

CONCLUSIONS

A convenient eco-friendly, low-cost solvothermal synthetic strategy has been proposed to prepare spherical magnetite nanoparticles of different sizes with low polydispersity. The hydrolysis and condensation reactions of the iron alkoxide at the basis of the formation of the iron oxide are controlled by varying the ratio between the iron precursor and the surfactants (oleic acid and oleylamine), the ratio between the two surfactants, as well as the reaction temperature. A linear trend has been found both for particle size and crystallite size as a function of temperature. An in-depth study on the role of each surfactant has pointed out the fundamental role of the amine as reduction promoter as demonstrated by using different amines and confirmed by Mössbauer measurements. New insights in the reactions involved in the synthesis are provided. Oleic acid and oleylamine react forming a dialkylamide that constitutes a new surfactant and the actual capping agent of the nanoparticles. Furthermore,^{1}H-NMR data strongly suggest that the amide is bound at

the surface of the nanoparticles (both magnetite and anatase) through the amide proton (NH) probably via hydrogen bond, while oxygen and nitrogen are not directly involved. Water generated in situ from the condensation reaction, together with the vapour water used as the hydrolysis agent, react with the iron precursor to produce the final metal oxide. Considering the great importance of the amide bond in natural and synthetic compounds, the proposed solvothermal approach could be promising to prepare a great variety of hybrid inorganic-organic nanoparticles. In addition, the simultaneous use of titanium and iron alkoxides could lead to novel titanium-iron oxides composite materials.

ACKNOWLEDGEMENTS

Consorzio AUSI (Consorzio per la promozione delle Attività Universitarie del Sulcis-Iglesiente) is gratefully acknowledged for the grant financing for Claudio Cara. The use of the HRTEM facilities of C.G.S. (Centro Grandi Strumenti, University of Cagliari) is gratefully acknowledged. Thanks are due to Regione Autonoma della Sardegna (L.R. 7/2007) for the fellowships of A. Ardu. INPS (IstitutoNazionale di PrevidenzaSociale) Gestione ex-INPDAP is acknowledged with thanks for the grant financing for Valentina Mameli. This work is also supported by the Project GACR No.14-18392S.

SUPPORTING INFORMATION

Additional information over all conducted experiments. This material is available free of charge via the Internet at http://pubs.acs.org.

NOTES AND REFERENCES

(1) Niederberger, M.; Pinna, N. *Metal Oxide Nanoparticles in Organic Solvents. Synthesis, Formation, Assembly and Application*; Springer, 2009.

(2) Feng, S.; Xu, R. *Acc. Chem. Res.* **2001**, *34* (3), 239–247.

(3) Caruntu, D.; Caruntu, G.; O'Connor, C. J. In *Advanced wet-chemical synthetic approaches to inorganic nanostructures*; Cozzoli, P. D., Ed.; Transworld Research Network, 2008; pp 151–155.

(4) Tian, Y.; Yu, B.; Li, X.; Li, K. *J. Mater. Chem.* **2011**, *21* (8), 2476.

(5) Dinh, C.; Nguyen, T.; Kleitz, F.; Do, T. *ACS Nano* **2009**, *3* (11), 3737–3743.

(6) D'Arienzo, M.; Carbajo, J.; Bahamonde, A.; Crippa, M.; Polizzi, S.; Scotti, R.; Wahba, L.; Morazzoni, F. *J. Am. Chem. Soc.* **2011**, *133* (44), 17652–17661.

(7) Wang, X.; Zhuang, J.; Peng, Q.; Li, Y. *Nature* **2005**, *437* (7055), 121–124.

(8) Repko, A.; Nižňanský, D.; Poltierová-Vejpravová, J. *J. Nanoparticle Res.* **2011**, *13* (10), 5021–5031.

(9) Repko, A.; Nižňanský, D.; Matulková, I.; Kalbáč, M.; Vejpravová, J. *J. Nanoparticle Res.* **2013**, *15* (7), 1767.

(10) Murray, C. B.; Norris, D. J.; Bawendi, M. G. *J. Am. Chem. Soc.* **1993**, *115*, 8706–8715.

(11) De Mello Donegá, C.; Liljeroth, P.; Vanmaekelbergh, D. *Small* **2005**, *1* (12), 1152–1162.

(12) Riha, S. C.; Parkinson, B. A.; Prieto, A. L. *J. Am. Chem. Soc.* **2009**, *131* (34), 12054–12055.

(13) Pan, D.; An, L.; Sun, Z.; Hou, W.; Yang, Y.; Yang, Z.; Lu, Y. *J. Am. Chem. Soc.* **2008**, *130* (17), 5620–5621.

(14) Hessel, C. M.; Pattani, V. P.; Rasch, M.; Panthani, M. G.; Koo, B.; Tunnell, J. W.; Korgel, B. A. *Nano Lett.* **2011**, *11* (6), 2560–2566.

(15) Kwon, S. G.; Hyeon, T. *Acc. Chem. Res.* **2008**, *41* (12), 1696–1709.

(16) Park, J.; Joo, J.; Kwon, S. G.; Jang, Y.; Hyeon, T. *Angew. Chem. Int. Ed. Engl.* **2007**, *46* (25), 4630–4660.

(17) Park, S.; Kim, S.; Lee, S.; Khim, Z. G.; Char, K.; Hyeon, T. *J. Am. Chem. Soc.* **2000**, *122* (35), 8581–8582.

(18) Hyeon, T.; Lee, S. S.; Park, J.; Chung, Y.; Na, H. B. *J. Am. Chem. Soc.* **2001**, *123* (51), 12798–12801.

(19) Sun, S.; Zeng, H.; Robinson, D. B.; Raoux, S.; Rice, P. M.; Wang, S. X.; Li, G. *J. Am. Chem. Soc.* **2004**, *126*, 273–279.

(20) Hou, Y.; Yu, J.; Gao, S. *J. Mater. Chem.* **2003**, *13* (8), 1983.

(21) Lu, J.; Chen, D.; Jiao, X. *J. Colloid Interface Sci.* **2006**, *303* (2), 437–443.

(22) Kim, H.-J.; Choi, K.-I.; Pan, A.; Kim, I.-D.; Kim, H.-R.; Kim, K.-M.; Na, C. W.; Cao, G.; Lee, J.-H. *J. Mater. Chem.* **2011**, *21* (18), 6549.

(23) Sun, C.; Li, H.; Zhang, H.; Wang, Z.; Chen, L. *Nanotechnology* **2005**, *16* (9), 1454–1463.

(24) Wen, B.; Huang, Y.; Boland, J. J. *J. Phys. Chem. C* **2008**, *112* (1), 106–111.

(25) Ghoshal, T.; Maity, T.; Senthamaraikannan, R.; Shaw, M. T.; Carolan, P.; Holmes, J. D.; Roy, S.; Morris, M. a. *Sci. Rep.* **2013**, *3*, 2772.

(26) Ghosh, P.; Mandal, A.; Subba, R. *Catal. Commun.* **2013**, *41*, 146–152.

(27) Mattisson, T.; Johansson, M.; Lyngfelt, A. *Energy & Fuels* **2004**, *18* (3), 628–637.

(28) Zhao, N.; Ma, W.; Cui, Z.; Song, W.; Xu, C.; Gao, M. *ACS Nano* **2009**, *3* (7), 1775–1780.

(29) Magnacca, G.; Allera, A.; Montoneri, E.; Celi, L.; Benito, D. E.; Gagliardi, L. G.; Gonzalez, M. C.; Mártire, D. O.; Carlos, L. *ACS Sustain. Chem. Eng.* **2014**, *2* (6), 1518–1524.

(30) Chandra, V.; Park, J.; Chun, Y.; Lee, J. W.; Hwang, I.; Kim, K. S. *ACS Nano* **2010**, *4* (7), 3979–3986.

(31) Ali, I. *Chem. Rev.* **2012**, *112* (10), 5073–5091.

(32) Krishnan, K. M. *IEEE Trans. Magn.* **2010**, *46* (7), 2523–2558.

(33) Laurent, S.; Forge, D.; Port, M.; Roch, A.; Robic, C.; Vander Elst, L.; Muller, R. N. *Chem. Rev.* **2008**, *108* (6), 2064–2110.

(34) Roca, a G.; Costo, R.; Rebolledo, a F.; Veintemillas-Verdaguer, S.; Tartaj, P.; González-Carreño, T.; Morales, M. P.; Serna, C. J. *J. Phys. D. Appl. Phys.* **2009**, *42* (22), 224002.

(35) Thanh, N. T. K.; Green, L. a. W. *Nano Today* **2010**, *5* (3), 213–230.

(36) Hervault, A.; Thanh, N. T. K. *Nanoscale* **2014**, *6* (20), 11553–11573.

(37) Gupta, A. K.; Gupta, M. *Biomaterials* **2005**, *26* (18), 3995–4021.

(38) Ho, D.; Sun, X.; Sun, S. *Acc. Chem. Res.* **2011**, *44* (10), 875–882.

(39) Thanh, N. T. K.; Maclean, N.; Mahiddine, S. *Chem. Rev.* **2014**, *114* (15), 7610–7630.

(40) Zhai, X.; Zhang, X.; Chen, S.; Yang, W.; Gong, Z. *Colloids Surfaces A Physicochem. Eng. Asp.* **2012**, *409*, 126–129.

(41) Pérez-Mirabet, L.; Solano, E.; Martínez-Julián, F.; Guzmán, R.; Arbiol, J.; Puig, T.; Obradors, X.; Pomar, A.; Yáñez, R.; Ros, J.; Ricart, S. *Mater. Res. Bull.* **2013**, *48* (3), 966–972.

(42) Mourdikoudis, S.; Liz-Marzán, L. M. *Chem. Mater.* **2013**, *25* (9), 1465–1476.

(43) Xu, Z.; Shen, C.; Hou, Y.; Gao, H.; Sun, S. *Chem. Mater.* **2009**, *21* (9), 1778–1780.

(44) Carenco, S.; Boissière, C.; Nicole, L.; Sanchez, C.; Le Floch, P.; Mézailles, N. *Chem. Mater.* **2010**, *22* (4), 1340–1349.

(45) Nam, K. M.; Shim, J. H.; Ki, H.; Choi, S.-I.; Lee, G.; Jang, J. K.; Jo, Y.; Jung, M.-H.; Song, H.; Park, J. T. *Angew. Chem. Int. Ed. Engl.* **2008**, *47* (49), 9504–9508.

(46) Mondini, S.; Ferretti, A. M.; Puglisi, A.; Ponti, A. *Nanoscale* **2012**, *4* (17), 5356–5372.

(47) Schneider, C. A.; Rasband, W. S.; Eliceiri, K. W. *Nat. Methods* **2012**, *9* (7), 671–675.

(48) Ogg, R. J.; Kingsley, R. B.; Taylor, J. S. *J. Magn. Reson. Ser. B* **1994**, *104* (1), 1–10.

(49) Smallcombe, S. H.; Patt, S. L.; Keifer, P. A. *J. Magn. Reson. Ser. A* **1995**, *117* (2), 295–303.

(50) Chen, L.; Yang, X.; Chen, J.; Liu, J.; Wu, H.; Zhan, H.; Liang, C.; Wu, M. *Inorg. Chem.* **2010**, *49* (c), 8411–8420.

(51) Gaspa, S.; Porcheddu, A.; De Luca, L. *Org. Biomol. Chem.* **2013**, *11* (23), 3803–3807.

(52) Soulé, J.-F.; Miyamura, H.; Kobayashi, S. *J. Am. Chem. Soc.* **2011**, *133* (46), 18550–18553.

(53) Jing, Z.; Wu, S. *Mater. Lett.* **2004**, *58* (27-28), 3637–3640.

(54) Khalil, M.; Yu, J.; Liu, N.; Lee, R. L. *Colloids Surfaces A Physicochem. Eng. Asp.* **2014**, *453*, 7–12.

(55) Murad, E.; Johnston, J. H. In *Mössbauer Spectroscopy Applied to Inorganic Chemistry*; 1985; pp 507–583.

(56) Cornell, R. M.; Schwertmann, U. *The Iron Oxides*; Wiley-VCH Verlag GmbH & Co. KGaA: Weinheim, FRG, 2003.

(57) Morales, M. P.; Serna, C. J.; Bødker, F.; Mørup, S. *J. Phys. Condens. Matter* **1997**, *9* (25), 5461–5467.

(58) Kubelka, J.; Keiderling, T. A. *J. Phys. Chem. A* **2001**, *105* (48), 10922–10928.

(59) Cannas, C.; Musinu, A.; Ardu, A.; Orrù, F.; Peddis, D.; Casu, M.; Sanna, R.; Angius, F.; Diaz, G.; Piccaluga, G. *Chem. Mater.* **2010**, *22* (11), 3353–3361.

(60) Klokkenburg, M.; Hilhorst, J.; Erné, B. H. *Vib. Spectrosc.* **2007**, *43* (1), 243–248.

(61) Bu, W.; Chen, Z.; Chen, F.; Shi, J. *J. Phys. Chem. C* **2009**, *113* (28), 12176–12185.

(62) Rao, C. N. R. *Chemical Applications of Infrared Spectroscopy*; 1963.

(63) Muthirulan, P.; Devi, C. N.; Sundaram, M. M. *Ceram. Int.* **2014**, *40* (4), 5945–5957.

(64) Scorciapino, M. A.; Sanna, R.; Ardu, A.; Orrù, F.; Casu, M.; Musinu, A.; Cannas, C. *J. Colloid Interface Sci.* **2013**, *407*, 67–75.

(65) Mohamed, M. B.; AbouZeid, K. M.; Abdelsayed, V.; Aljarash, A. A.; El-Shall, M. S. *ACS Nano* **2010**, *4* (5), 2766–2772.

Tables

Table 1. Synthetic conditions

Samples*	FeIS (mmol)	Am[§] (mmol)	OAc (mmol)	FeIS/Am/OAc	Hydrolysis agent[+]
H_NS	0.530	-	-	1/0/0	EtOH
H_OAc	0.530	-	10.677	1/0/20	EtOH
M_OAm	0.530	15.902	-	1/30/0	EtOH
M1_ OAm _OAc	0.530	3.180	2.12	1/6/4	EtOH
M2_OAm_OAc	0.530	15.902	10.677	1/30/20	EtOH
M3_ OAm_OAc	0.530	15.902	10.677	1/30/20	-
M2_BuAm_OAc	0.530	15.902	10.677	1/30/20	EtOH
M2_OcAm_OAc	0.530	15.902	10.677	1/30/20	EtOH
M2_OAm	0.530	0.530	-	1/1/0	EtOH
M2_OcAm	0.530	0.530	-	1/1/0	EtOH
M2_BuAm	0.530	0.530	-	1/1/0	EtOH

*All the samples have been prepared using Absolute Ethanol as solvent (total volume of the mixture 15 mL) and a temperature of 180°C for 18 hours.

[§] Am = amine (OAm:Oleylamine; OcAm: Octylamine; BuAm: Bytilamine)

[+] The hydrolysis agent is the azeotropic mixture ethanol /water 96.4%

Table 2. Crystallite size ($\langle D \rangle_{XRD}$) and Particle size ($\langle D \rangle_{TEM}$) of the samples obtained at different temperatures

Samples	*T_R (°C)	$\langle D \rangle_{XRD}$ (nm)	$\langle D \rangle_{TEM}$ (nm)	Polidispersity. s.d. %
M2_T140	140	4.2±0.4	7.4	21
M2_T160	160	5.7±0.5	7.2	8
M2_T180[+]	180	6.5±0.3	8.5	9
M2_T200	200	6.9±0.4	9.8	10
M2_T220	220	8.73±0.3	11.5	8

***T_R :**Reaction Temperature; [+] M2_T180 corresponds to M2_OAm_OAc

Table 3. Mössbauer Parameters of the Samples M2_OAm_OAc and M2_BuAm_OAc at Room Temperature: Values of Isomer Shift (δ) Half-Width at Half-Maximum (Γ/2), Hyperfine Magnetic Field (B), and Relative Area (A) of the Components

Sample	Components	δ	ΔE_Q	B_{Hf}	Γ/2 [mm/s]	A (%)	Interpretation
M2_OAm_OAc	Sextet 1	0,26	-0,04	48,8 T	0,28	32	Fe^{3+} in tetrahedral position in magnetite
	Sextet 2	0,68	-0,01	45,7 T	0,68	68	Fe^{2+} and Fe^{3+} in octahedral position in magnetite
	Singlet	0.36	-	-	2.26	-	Fe^{3+} in non ordered state /superparamagnetic
M2_BuAm_OAc	Sextet 1	0,29	-0,04	48,9 T	0,22	35	Fe^{3+} in tetrahedral position in magnetite
	Sextet 2	0,65	-0,01	45,7 T	0,34	65	Fe^{2+} and Fe^{3+} in octahedral position in magnetite
	Singlet 3	0.35	-	-	1,28	-	Fe^{3+} in non ordered state /superparamagnetic
	Singlet 4	0,36	-	-	6,91	-	Fe^{3+} in non ordered state /superparamagnetic

Table 4**.** ^{1}H-NMR resonances assignment, multiplicity and relative integrated area.

	^{1}H chemical shift [ppm] (multiplicity[a]; relative integrated area[b])				
Samples	**HN** (amide)	**-CαH$_2$**-NH- (amide)	**-CαH$_2$**-NH- (OAm)	**-CαH$_2$**-CO- (OAc)	-CO-**CαH$_2$**- (amide)
OAm			2.564 (t; ---)		
OAc				2.179 (t; ---)	
OAm_OAc	absent	absent	2.678 (t; ---)	2.059 (t; ---)	absent
W_M2_OAm_OAc	7.900 (t; 1.00)	3.088 (dt; 1.13)	2.577 (t; 1.87)	2.208 (t; 0.34)	2.100 (t; 1.26)
A_OAm_OAc_W	7.456 (t; 1.00)	3.125 (dt; 1.06)	absent	absent	2.109 (t; 1.18)
W_A_OAm_OAc	7.899 (t; 1.00)	3.087 (dt; 1.09)	2.570 (t; 0.98)	2.207 (t; 0.04)	2.095 (t; 1.15)

[a]dt: doublet of triplets; t: triplet.

[b] Integrals are referred to the amide proton resonance in the same spectrum.

Figures

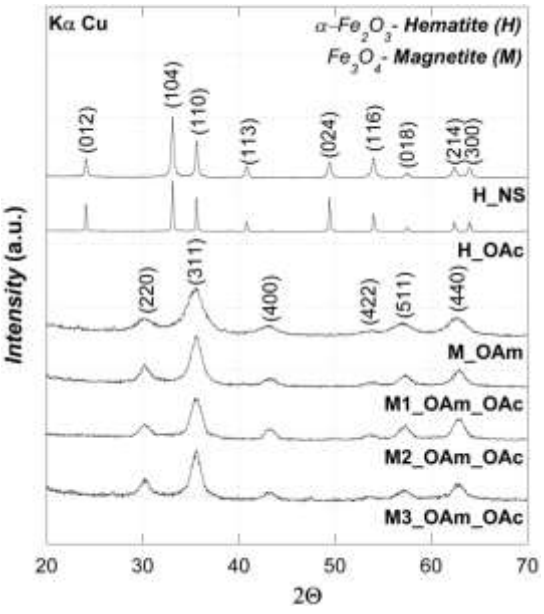

Figure 1. XRD patterns of the samples prepared in different synthetic conditions (see Table 1)

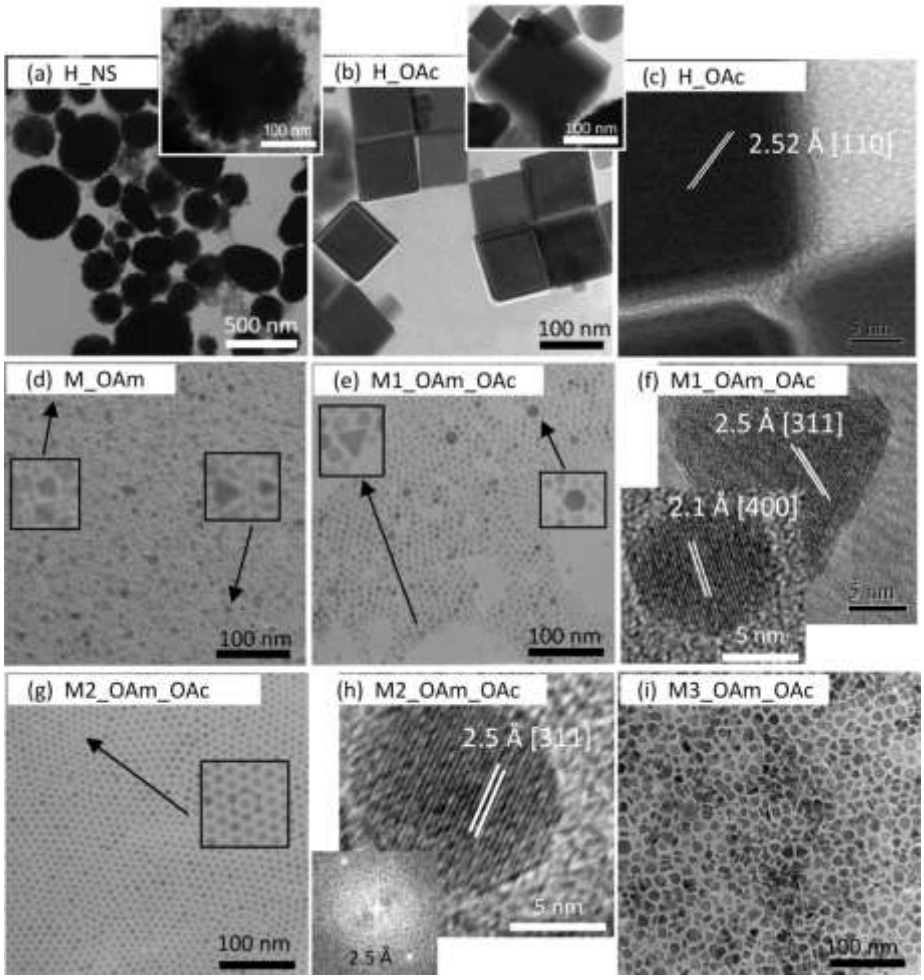

Figure 2. TEM and HRTEM images of the samples prepared in different synthetic conditions (see Table 1)

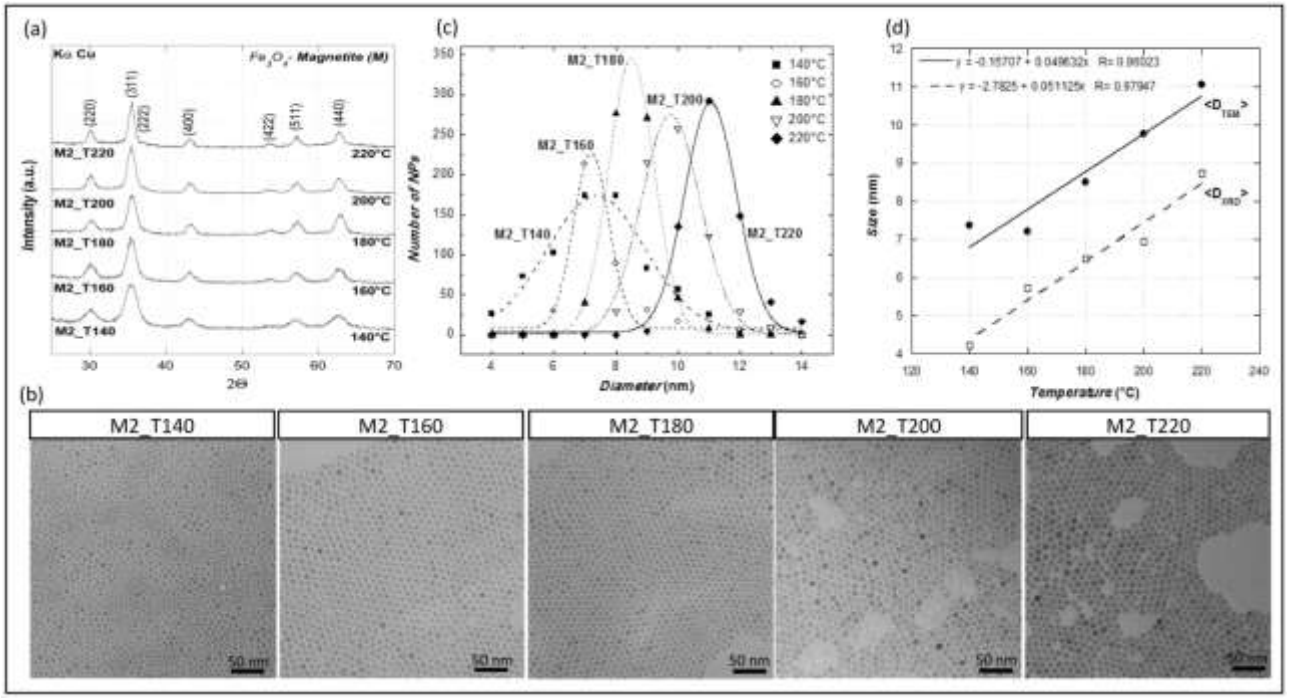

Figure 3. XRD patterns (a), TEM bright images (b), Particle Size Distributions (c) and D_{XRD} and D_{TEM} size versus temperature (d) of the samples obtained in the same synthetic conditions of M2_OAc_OAm = M2_T180 (see Table 1) at different reaction temperatures.

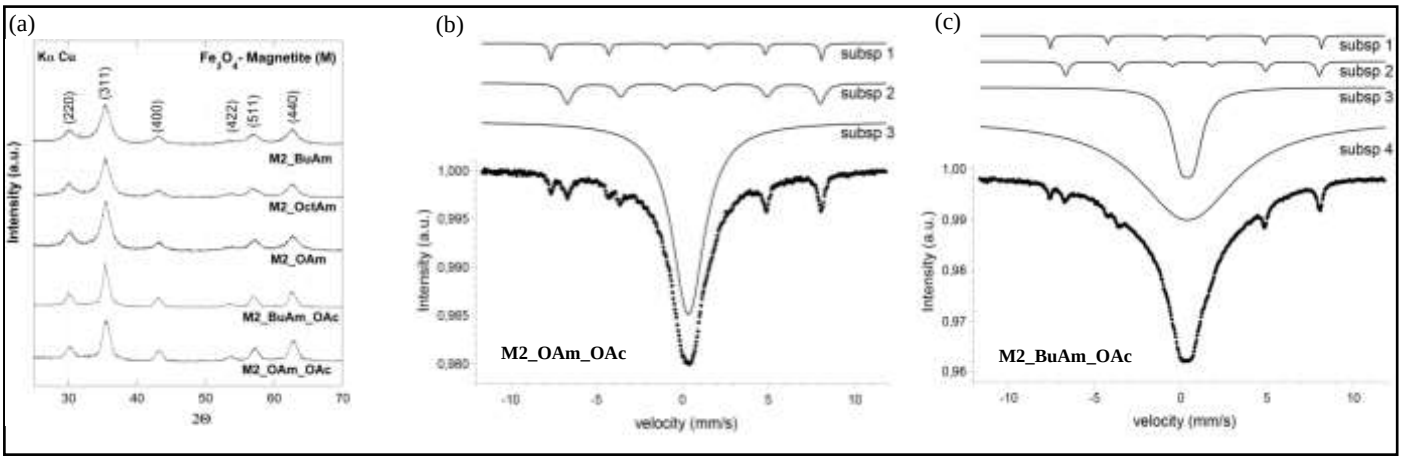

Figure 4. XRD patterns (a) of the sample prepared with different amines and RT Mössbauer Spectra of the samples M2_OAm_ OAc (b) and M2_BuOAm_OAc (c), (see Table 1 and Table 3)

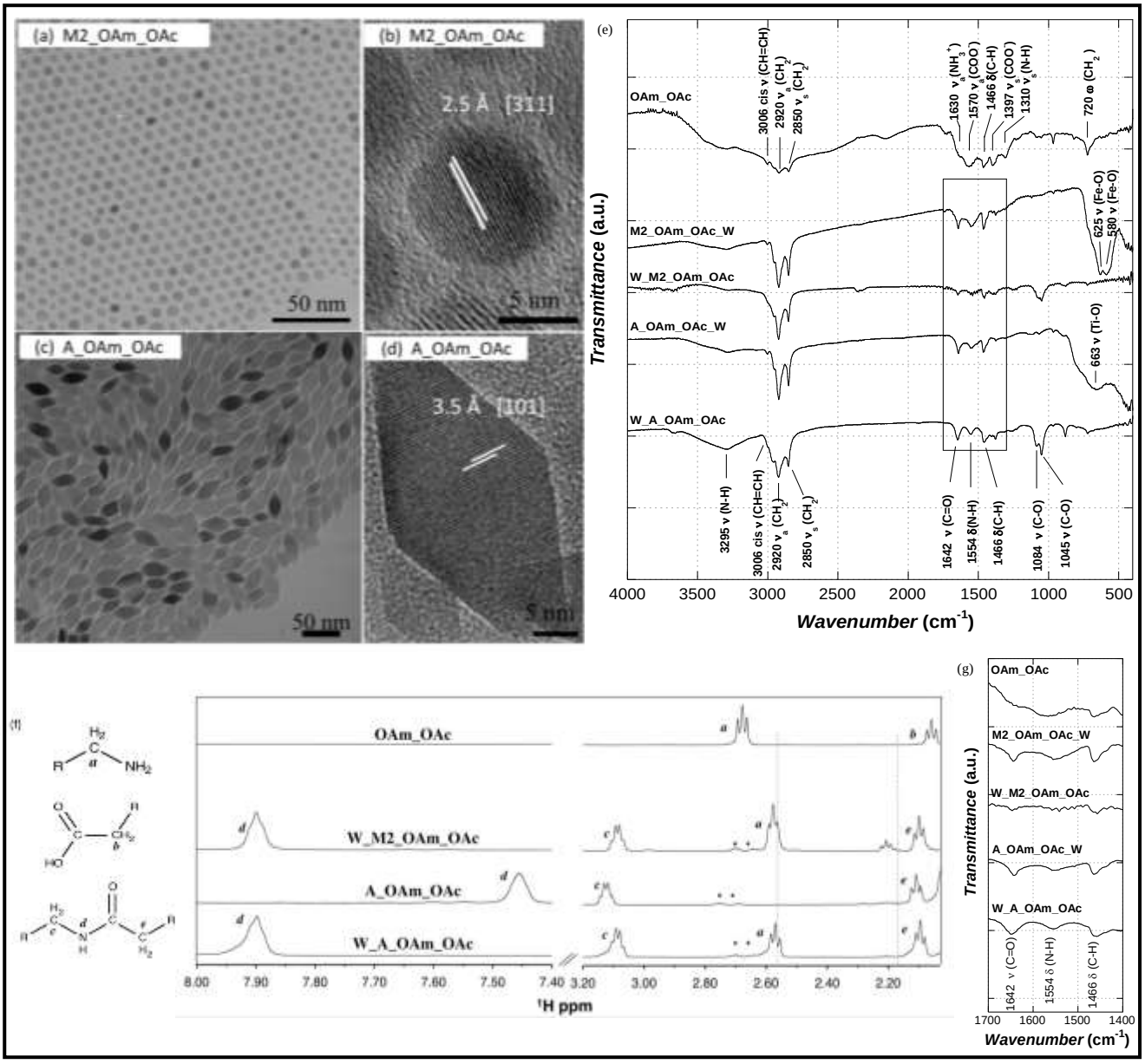

Figure 5. TEM and HRTEM images of magnetite (M2_OAm-OAc) (a,b) andanatase (A_OAm_OAc) (c,d) colloidal dispersions. FTIR of magnetite (M2_Aom_OAc) and anatase (A_OAm_OAc) colloidal dispersions with the relative washing solutions (W_M2_Aom_OAc, W_A_OAm_OAc) (e). One-dimensional ^{1}H-NMR spectrum anatase dispersion (A_OAm_OAc) and the washing solutions of magnetite and anatase samples (W_M2_Aom_OAc, W_A_OAm_OAc) (f). FTIR and ^{1}H-NMR spectra of a mixture of OAc and OAm at room temperature are reported as references. The two vertical dashed lines at 2.56 and 2.18 ppm indicate the position of CαH$_2$ from OAm and OAc, respectively, when separately dissolved in ethanol. Asterisks are used to indicate impurities coming from commercial OAm (maximum purity available 70%). (g) Inset of the FTIR spectra showing the typical vibration mode of the amide.

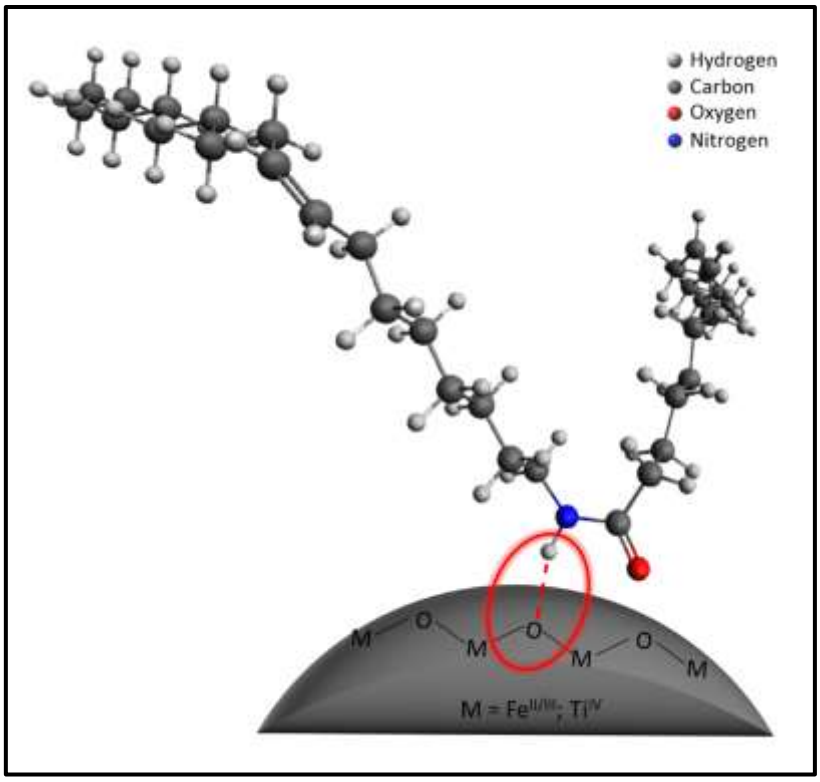

Figure 6. Schematic representation of the dialkylamide-capped nanoparticles (magnetite and anatase).